AAPS PharmSciTech, Vol. 9, No. 2, June 2008 (© 2008)
DOI: 10.1208/s12249-008-9104-2

Research Article

Behavior of Freezable Bound Water in the Bacterial Cellulose Produced by *Acetobacter xylinum*: An Approach Using Thermoporosimetry

Sanae Kaewnopparat,[1] Kamonlawat Sansernluk,[2] and Damrongsak Faroongsarng[1,3]

Received 4 March 2008; accepted 10 April 2008; published online 4 June 2008

Abstract. The aim of the study is to examine thermal behavior of water within reticulated structure of bacterial cellulose (BC) films by sub-ambient differential scanning calorimetry (DSC). BC films with different carbon source, either manitol (BC (a)) or glycerol (BC (b)), were produced by *Acetobacter xylinum* using Hestrin and Shramm culture medium under static condition at 30±0.2°C for 3 days. BC samples were characterized by electron scanning microscopy and X-ray diffraction spectroscopy. The pore analysis was done by B.H.J. nitrogen adsorption. The pre-treated with 100% relative humidity, at 30.0±0.2°C for 7 days samples were subjected to a between 25 and −150°C-cooling–heating cycle of DSC at 5.00°C/min rate. The pre-treated samples were also hydrated by adding 1 μl of water and thermally run with identical conditions. It is observed that cellulose fibrils of BC (a) were thinner and reticulated to form slightly smaller porosity than those of BC (b). They exhibited slightly but non-significantly different crystalline features. The freezable bound water behaved as a water confinement within pores rather than a solvent of polymer which is possible to use thermoporosimetry based on Gibb–Thomson equation to approach pore structure of BC. In comparison with nitrogen adsorption, it was found that thermoporosimetry underestimated the BC porosity, i.e., the mean diameters of 23.0 nm *vs.* 27.8 nm and 27.9 nm *vs*. 33.9 nm for BC (a) and BC (b), respectively, by thermoporosimetry *vs.* B.H.J. nitrogen adsorption. It may be due to large non-freezable water fraction interacting with cellulose, and the validity of pore range based on thermodynamic assumptions of Gibb–Thomson theory.

KEY WORDS: *Acetobacter xylinum*; bacterial cellulose; Gibb–Thomson equation; melting point depression; thermoporosimetry.

INTRODUCTION

Cellulose, a linear β-1, 4-linked glucose polymer is the most abundant natural biopolymer on Earth. In addition to plants which are major sources, some acetic acid bacteria for example, *Acetobacter xylinum* could produce cellulose. The bacterial cellulose (BC) is markedly different from plant counterpart. It consists of the pure cellulose network made up of a random assembly of ribbon shaped fibers free of lignin and hemicelluloses (1). As BC provides unique properties such as high values in Young's modulus, sonic velocity (2), and water sorption capacity (3), it has been receiving much attention in biomedical applications. For instance, BC is an interesting material for using as a wound dressing since it maintains the proper moisture level of wound bed and protects the wound against contamination. Its proper moisture content could accelerate healing, activate autolytic debridement of the wound, and facilitate angiogenesis and re-epithelization (4).

Water sorption with cellulose has been proposed to present in three distinct fractions: (1) non-freezable bound water, (2) freezable bound water, and (3) free or bulk water (5). Freezable bound water always freezes at temperature below 0°C. Thermodynamically, this phenomenon governs by two different processes, i.e., either polymer solution or water confinement within reticulated structure of cellulose. On one hand, it has been demonstrated that the depressed melting temperature of a fraction of bound water in hydrogels of some cellulose derivatives may be due to polymer solution (6). On the other hand, previous study in microcrystalline cellulose–water interaction suggested that bound water may reside in small pores created during wet granulation resulting in lowering its phase transition temperature (7). And, water present in the BC gels may be confined in reticulated structure rather than forming a continuous phase throughout the gel (8). Furthermore, it was demonstrated that only 10% of the 99% water present in BC gels behave like free bulk water, i.e., the majority of the water molecules in the gels is more or less tightly bound to the cellulose (8). Thus, bound water in BC is of interest as it may play an important role in wound healing mechanism. In addition, the reticulated structure characterization of BC film becomes important due to the fact that some agents such as silver nanoparticles (4) have been incorporated in BC to have the wound dressing with antimicrobial activity. Thermal behavior of water may characterize the reticulated

[1] Drug Delivery Systems Research Center, Department of Pharmaceutical Technology, Faculty of Pharmaceutical Sciences, Prince of Songkla University, Hat Yai, 90112, Thailand.
[2] Department of Pharmaceutical Technology, Faculty of Pharmaceutical Sciences, Prince of Songkla University, Hat Yai, 90112, Thailand.
[3] To whom correspondence should be addressed. (e-mail: damrongsak.f@psu.ac.th)

structure of BC membranes as the interfacial tension related to surface of curvature of water within pores could develop and then depress the water confinement phase transition (6). The aim of this study is to examine the thermal behavior of freezable bound/confined water within reticulated structure of BC films by sub-ambient differential scanning calorimetry with an approach using thermoporosimetry.

MATERIALS AND METHODS

Lyophilized form of *A. xylinum* TISTR 975 was purchased from Thailand Institute of Science and Technology Research, Bangkok. Hestrin and Shramm (9) medium (HS) was used as a medium for bacterial culture. Lyophilized *A. xylinum* was suspended in HS broth and incubated at 30±0.2°C for 3 days. The cell suspension was preserved with 20% glycerin and stored at −80°C prior to use.

Bacterial Cellulose (BC) Production

To cultivate bacterial celluloses, *A. xylinum* TISTR 975 cell suspension was cultured with static condition. The method of bacterial culture was previously described (10). The details in brief are as follows: The preserved cell suspension was sub-cultured in HS broth two times and then on HS agar with 3-day incubation period at 30±0.2°C for each step. The bacteria colonies on agar surface were collected and sugar free HS broth was added to make the turbidity of suspension equal to McFarland no. 1 turbidity standard or $\sim 4.5 \times 10^7$ CFU/ml. Stray cellulose fibers produced during bacteria growth were removed. This standardized cell suspension was individually cultured on HS medium containing 8% w/v either manitol (BC (a)) or glycerol (BC (b)) as a carbon source. Five ml of cell suspension was added to 50 ml medium in a 1,000 ml-beaker with cross sectional area of 63.6 cm^2, and incubated at 30± 0.2°C for 3 days under static condition. BC produced by *A. xylinum* accumulated at the surface of the culture medium as a gelatinized membrane. The BC films were harvested and washed with running water. They were consecutively immersed in 2% w/v sodium hydroxide for 24 h and 0.1% w/v sodium hyperchlorite for another 24 h, and then washed with distilled water for several times. Finally, clean BC films were dried at 50°C (hot air oven) for 24 h.

Morphologic Study and Structural Features of BC

For morphologic observation, scanning electron micrographs of BC membranes were obtained (SEM, JEOL Ltd., Tokyo, Japan). Prior to the examination, the samples were gently fixed on an aluminum stab with two-side adhesive tape, and coated with 15–20 nm thick layer of gold. The structural features of BC were done by X-ray diffraction study. The X-ray diffraction patterns (XRD) were recorded in a Philips: X'Pert MPD diffractometer (Philips Analytical, Eindhoven, The Netherlands) using copper-Kα as a radiation source. The traces were recorded over a range of 5–40° (2θ angle). The structural feature parameters including crystallinity index, Crystallite size, and Difference in Bragg angle were calculated from XRD patterns using the method previously described by Watanabe *et al.* (2).

Reticulated Pore Analysis of BC by Nitrogen Adsorption

The nitrogen adsorption method was employed to determine pore size and distribution of obtained BC. Accurately weighted dry samples were put in sample tubes and outgased at 90°C for 3 h to rid surface moisture and other contaminants. The samples were then subjected to automatic surface area and pore size analyzer (Coulter SA3100, Backman Coulter, Inc., Fullerton, CA, USA). Sample tube free space was accurately measured using helium gas. Multi-point nitrogen adsorption isotherms of BC (a) and BC (b) were obtained at 77 K. Barret–Joyner–Halenda (B.H.J.) pore size analysis was done by Coulter software version 2.13 (Backman Coulter, Inc., Fullerton, CA, USA).

Sub-ambient Differential Scanning Calorimetric Study of Water Sorption on BC

The samples were pre-treated with 100% relative humidity at 30.0±0.2°C for 7 days prior to DSC analyses. The Perkin-Elmer differential scanning calorimeter (DSC7 with TAC7/DX Thermal analysis controller, Perkin-Elmer Corp., Norwalk, CT, USA) equipped with liquid nitrogen bath set as a cooling accessory was employed. Calibrations with Indium and cyclohexane were carried out for every time which the DSC operation started to ensure the accuracy/precision of the obtained heat of transitions and the corresponding temperatures. An accurately weighed (5–15 mg) sample was placed in tightly sealed aluminum pan (Perkin-Elmer Corp., Norwalk, CT, USA). The samples were subjected to run against an empty pan as a reference. With loading temperature of 25°C, the analysis program includes (1) cooling from 25°C to −150°C at 5.00°C/min rate, (2) isothermal run at −150°C for 1 min, and (3) heating from −150°C to 25°C at the same rate as cooling step. The pre-treated samples were also fully hydrated by adding 1 μl of liquid water and subjected to DSC run with identical conditions for those without liquid water added. All of DSC thermograms (cooling or heating traces) were analyzed using Pyris® software (Perkin-Elmer Corp., Norwalk, CT, USA).

RESULTS AND DISCUSSION

Bacterial Cellulose (BC) Membranes: Morphology and Structural Features

Dry weight, thickness, and production yield, of BC (a) and BC (b) having manitol and glycerol, respectively, as a carbon source are listed in Table I. Whereas, Fig. 1 shows the electron scanning photomicrographs of obtained BC (a) and BC (b) films. Both samples show the reticulated structure consisting of ultrafine cellulose fibrils. Even though, the membrane thicknesses were comparable, BC (b) is slightly heavier than BC (a) (Table I). As seen in Fig. 1, BC (a) exhibits somewhat thinner fibrils than BC (b). This might result in the dry weight difference. The cellulose fibrils rest on one another resulting in porosity formation. BC (a) apparently shows smaller pores compared with BC (b). It is thus demonstrated that *A. xylinum* cultured with different carbon sources could yield different sizes and

Table I. Dry Weight, Membrane Thickness, and Percent Yield of Obtained BC Membranes of 63.6 cm^2 Area

Obtained membrane properties	BC (a) Mean, S.D.	BC (b) Mean, S.D.
Dry weight (mg)	171, 1	203, 5
Thickness (μm)	32.0, 2.8	33.2, 1.9
*Yield (%)	2.14, 0.01	2.54, 0.06

*Yield=100×(dry weight BC/weight of carbon source)
The values were obtained from six replications. BC (a) and BC (b) are bacterial celluloses grown in HS media with manitol and glycerol was respectively used as carbon sources

weight of cellulose fibrils as well as reticulated porosities of the obtained film.

Figure 2 shows the XRD patterns for BC (a) and BC (b) which are apparently similar to each other. Diffraction peaks at 14.4° (labeled as 1 in Fig. 2) and 22.7° (labeled as 3 in Fig. 2) are assigned to the cellulose 1α and 1β phases which have previously been characterized by Barud *et al.* ($100_{1\alpha}$, $110_{1\beta}$ and $010_{1\beta}$ planes at ∼15° and $110_{1\alpha}$ and $200_{1\beta}$ at ∼22.5° (1)). It is common since the native cellulose from *A. xylinum* is rich in 1α-cellulose (8). The structural features derived from XRD including Crystallinity index, Crystallite size, and Difference in Bragg angle are tabulated in Table II. As seen in Table II, BC (a) has higher crystallinity index but smaller crystallite size of crystallographic plane (110) than BC (b). The difference in Bragg angle between peak 1 and 2 in Fig. 2 for BC (b) is less than that for BC (a) suggesting that BC (b) has a slightly lower content of cellulose 1α than BC (a). It is because there has been previously reported that (2): (1) the crystal transformation from cellulose 1α to cellulose 1β may result in the decrease in d-spacing with the shift of peak 1 to the wider angle that brings peak 1 closer to peak 2, and (2) Peak 2 may also shift to smaller angle, which brings peak 2 closer to peak 1, when the content of cellulose 1α decreases due to the difference in unit cells of cellulose 1α and cellulose 1β. It is possible that less content of cellulose 1α might result in less crystallinity index whereas larger crystallite size might cause larger fibrils of BC (b) illustrated in Fig. 1 and, in turn, reticulates larger pores than that of BC (a).

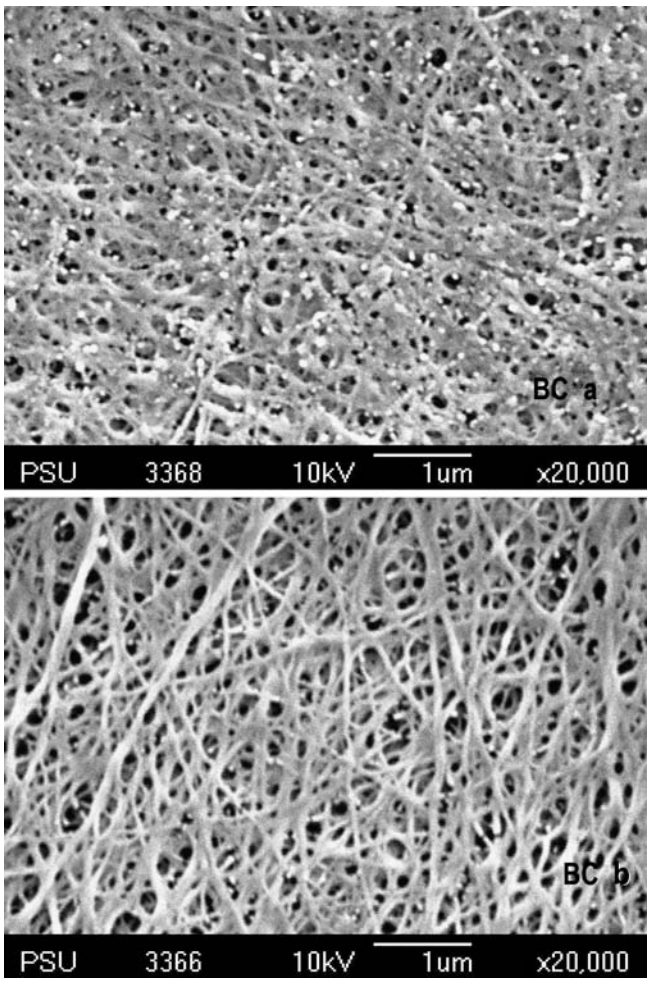

Fig. 1. Electron scanning photomicrographs of bacterial cellulose membranes having manitol: *BC a* and glycerol: *BC b* as a carbon source for culture medium

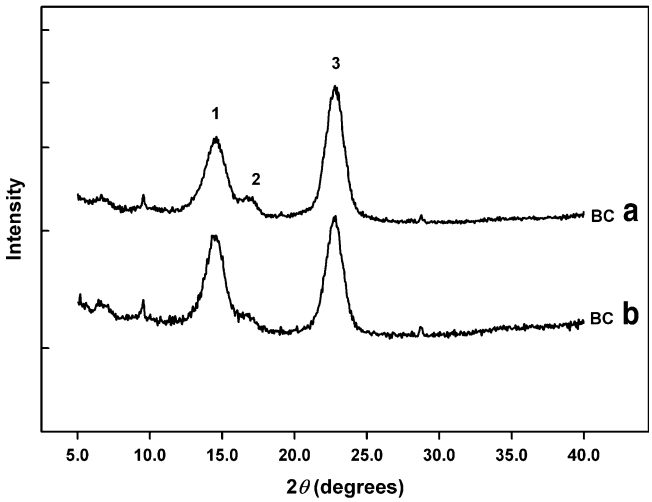

Fig. 2. X-ray diffraction patterns of cellulose crystalline of BC a and BC b membranes

Freezable Water Fractions on BC Membranes by DSC

Figure 3 illustrates the DSC cooling and heating traces of water sorption on a BC membrane labeled as traces I and II, respectively. It is noticed that both BC (a) and BC (b)

Table II. Structural Features of BC Membranes in Static Cultures with Different Carbon Sources

Structural feature	BC (a)	BC (b)
Crystallinity index* (%)	84.4	64.8
Crystallite size** (nm)	6.8	7.3
Difference in Bragg angle*** (°)	2.10	1.85

BC (a) and BC (b) are bacterial celluloses grown in HS media with manitol and glycerol was respectively used as carbon sources
*Calculated as the ratio of the area of the resolved crystalline peaks to the total area of a diffraction profile for 5–40° (2)
**Estimated as crystallite size of a crystallographic plane (110)
***Difference in Bragg angle between peak 1 and 2 in Fig. 2

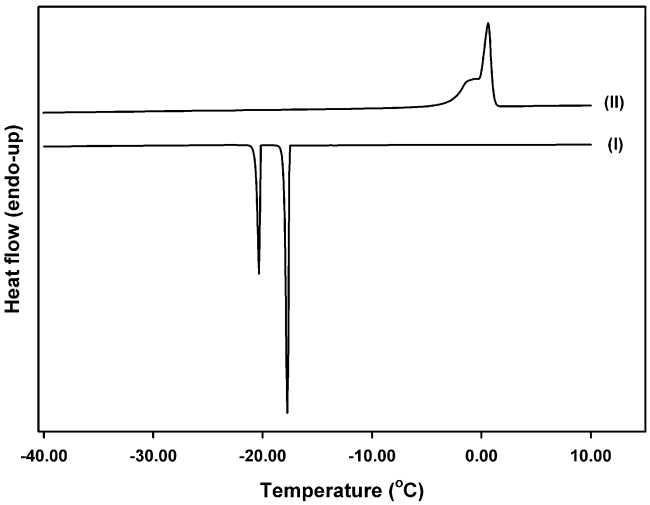

Fig. 3. Differential scanning calorimetric traces of water in the system of BC a equilibrated with 100% relative humidity. Key: (*I*): Cooling trace (*II*): Heating trace

show the DSC tracing in a similar pattern as demonstrated by Fig. 3. There are two fractions of freezable water where the solid–liquid transitions occur at below and closed to normal melting point which is consistent with previous studies (6,11). The trace which is closer to normal melting transition is free water whereas the other one is bound or confined water within film. It is noted that on one hand free water freezes at the temperature far below equilibrium freezing point (trace I in Fig. 3). On the other hand, it's melting shows up at a temperature slightly higher than zero (trace II in Fig. 3). Thus, the system exhibits either supercooling or superheating where water crystalline present in meta-stable states. It is known that supercooling or superheating phenomenon is influenced by surface tension fluctuation and the defects of the surface structure. Supercooling of the liquid phase in crystallization is proposed to be more difficult to retain stable nuclei in the present of defects than superheating of the solid in melting counterpart (12). As a result, the crystallization temperature of supercooling significantly deviates from the equilibrium transition compared with the melting point of superheating. It is also noted that two fractions of water melt in superheating at temperatures very close to each other while they well separately freeze in supercooling (Fig. 3). It may be because significant amount of bound or confined water becoming liquid phase during heating migrates from the vicinity of the sorption sites due to hydrogen bonding among water molecules to be in re-equilibrium with free fraction of water remaining on the surface of the membrane that melt later. This phenomenon is consistent with freezable bound water in other hydrophilic polymers (6).

Water Crystallization Thermoporosimetry for BC Membranes

The DSC tracing of bound or confined water has been proposed to be due either to water–polymer interaction (6) or to porosity confinement (11). The interpretation that which phenomenon is preference in BC (a) and BC (b) is essential so as not to mislead the further analysis. Although both phenomena allow water freezes/melts at sub-zero temperature, the resulting freezable bound water should behave differently. As mentioned by Faroongsarng and Sukonrat (6), if the porosity governs the freezing/melting point depression, then the depressed temperature in various moisture environments of the same material which would be similar pore structure may be invariant. Figure 4 shows the DSC cooling traces could be found on either BC (a) or BC (b) membrane. Traces I and II show the frozen water of BC equilibrated with 100% relative humidity with and without the addition of 1 μL water, respectively. As seen in Fig. 4, water crystallization traces behave in identical manner. Thus, the depressed temperature, i.e., the difference between transition temperatures of freezable free water and bound water fractions (ΔT) may be attributed to water confinement inside porosity of the BC membrane under study rather than polymer solution. This finding is consistent with the characterization of water in BC using dielectric spectroscopy and transmission electron microscopic images previously reported (8). It is then possible to utilize the DSC traces in Fig. 4 as the probes to examine the reticulated porosity of the BC (a) and BC (b) in the current study with the technique based upon Gibbs–Thomson equation where the interfacial tension related to surface of curvature of water within pores depress the phase transition of water:

$$\Delta T = T_p - T_0 = \frac{2\gamma\, Cos\theta T_0}{\Delta H_m \rho_s R_p} \quad (1)$$

Where, T_p is the melting temperature of liquid confined in a pore of radius R_p, T_0 is normal melting temperature of liquid, γ is surface energy of the solid/liquid interface. θ, ΔH_m, and ρ_s are contact angle, melting entropy, and density of solid phase, respectively. In addition, the cooling trace was selected because of a good resolution between freezable water fractions without migration out of the porous solid (trace I in Fig. 3).

As seen in Equation 1, the size of the pore where frozen water confined within is related to the depressed temperature

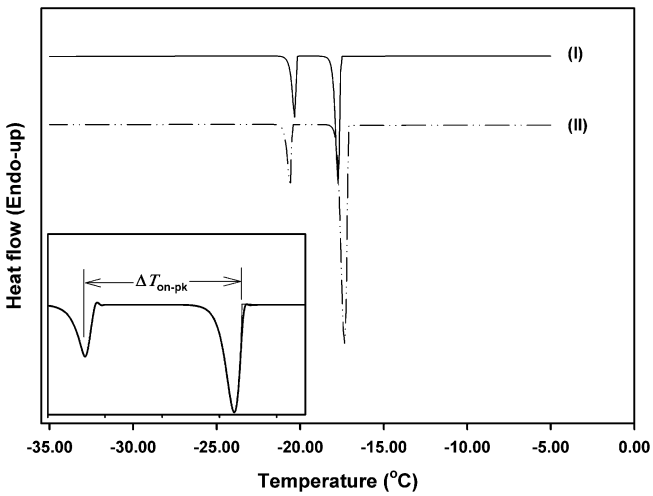

Fig. 4. DSC cooling trace of water sorption on BC b equilibrated with 100% relative humidity (*I*) and with 100% relative humidity with the addition of 1 μL water (*II*). *Inset* shows the "peak-onset" method of depressed temperature calculation

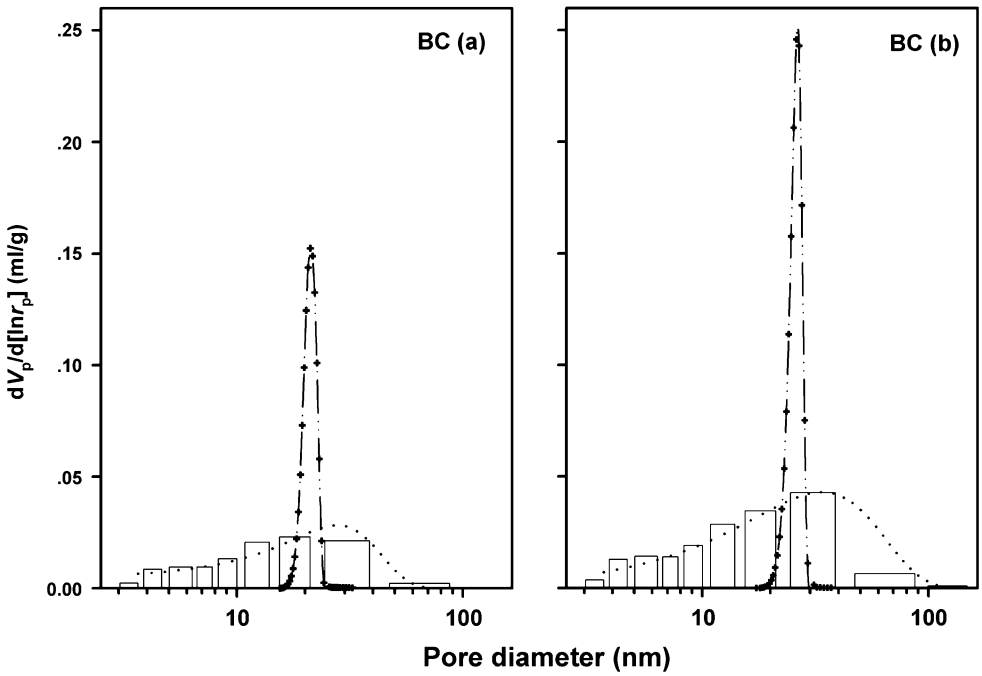

Fig. 5. Pore size distributions of BC a (*left hand side*) and BC b (*right hand side*) compared between water crystallization thermoporosimetry based on Gibb–Thomson equation (*broken line*) and B.H.J. nitrogen adsorption (*bars* and *dotted line*)

whereas it is found that the water transition lies upon supercooling or superheating that is usually not reproducible with any precision. The situation could bring the difficulty for reliable pore determination. Fortunately for each of the DSC runs, there is a freeze/melt transition of free water fraction that may presumably be in the same meta-stable conditions as the following confined one. The accompanying free water fraction tracing then serves as the reference to calculate the depressed temperature of confined fraction. The difference between confined fraction and extrapolated onset of the free fraction ($\Delta T_{\text{on-pk}}$) in absolute temperature scale based on "peak-onset" method described by Landry (13) as showed in the inset of Fig. 4 is currently in use. It is found that the pore size calculation is reproducible for the same BC with different water content.

In addition to supercooling/superheating phenomenon, freeze/melt hysteresis might also cause the difficulty in pore size determination by Equation 1. While supercooling/superheating deals with the inconsistency of free water crystallization/melting transition, the freeze/melt hysteresis concerns about the inconsistency of the magnitude of the depressed temperature between cooling and heating traces. It is seen in Fig. 3 that the difference in temperature between bound and free water upon solidification is larger than that of melting. Beside the migration of liquid phase discussed above, the hysteresis may be due to the difference in the curvature of a liquid–solid interface during the transformation process (14), as well as pore shape and geometry (13). To cope with the hysteresis, Ishikiriyama *et al.* (15) and Landry (13) have successfully used controlled pore glass samples with standard pore sizes and obtained the calibration equations for pore size conversion from depressed temperatures of both cooling and heating traces that written in general form as:

$$\Delta T_{on-pk} \frac{A}{r_p - \delta} + B \tag{2}$$

where, A and B are empirical constants, and δ is the thickness of non-freezable water adjacent to the pore wall

Table III. The Porosity Parameters Obtained from Water Crystallization Thermoporosimetry Based on Gibb–Thomson Equation of BC Membranes with Different Pore Sizes Compared with those Obtained from B.H.J. Nitrogen Adsorption

Parameter	BC (a)		BC (b)	
Method	[1]Nitrogen adsorption	[2]Thermoporosimetry	Nitrogen adsorption	Thermoporosimetry
V_p (cm^3/g)	0.114	0.079	0.128	0.118
S_p (m^2/g)	17.7	15.0	31.8	18.4
[3]D_{av}, *S.D.* (nm)	27.8, 14.1	23.0, 1.40	33.9, 47.7	27.9, 1.60

BC (a) and BC (b) are bacterial celluloses grown in HS media with manitol and glycerol was respectively used as carbon sources
[1] The data were obtained from nitrogen adsorption where V_{pp} was BET specific surface
[2] The results were obtained from pore distribution derived from DSC exotherm using equations 5 and 6
[3] D_{av} and S.D. are geometric means and standard deviations of pore distribution based on non-linear fitting

which is 1–2 molecular layers for cellulose fibers (16) for it is known that non-freezable bound water always present in a cellulose–water system (5). Equation 2 is useful since it is possible to extrapolate the temperature of crystallization of the solvent of the same type confined in a given pore without further calibration (17). However, the validity of Equation 2 is limited to the pore size range used for its determination especially for extrapolation towards large size of the pore. Landry's (13) calibration equation where the values of A and B are 38.558 and 0.1719 K, respectively, was selected in the current study because it covered appropriate range of pore sizes for BC (from 7.5 to 208.4 nm), and the δ of 0.3 nm was chosen for the molecular size of water (18). The heat flow ($\frac{dQ}{dt}$) of a DSC exotherm is converted to $\frac{dV_p}{dr_p}$ by equation 3 (13,15,17, and 19):

$$\frac{dV_p}{dr_p} = \frac{dQ}{dt}\frac{dt}{d(\Delta T)}\frac{d(\Delta T_{on-pk})}{dr_p}\frac{1}{m\Delta H_f(T)\rho(T)} \quad (3)$$

Where $\frac{d(\Delta T)}{dt}$ is the DSC scanning rate, m is mass of the dry membrane, and $\frac{d(\Delta T_{on-pk})}{dr_p}$ is the first derivative of equation 2. $\Delta H_f(T)$ and $\rho(T)$ are the temperature-dependent heat of fusion and density of ice governed by equations 4 and 5, respectively.

$$\Delta H_f(T) = 334.1 + 2.119(T - T_0) - 0.00783(T - T_0)^2 \quad (4)$$

$$\rho(T) = 0.917\left(1.032 - 1.17X_{10}^{-4}T\right) \quad (5)$$

And, the porosity parameters including total pore volume (V_p), and internal surface area (S_p) could be derived from the obtained distribution as follows:

$$V_p = \int_0^\infty \left[\frac{dV_p}{dr_p}\right] \cdot dr_p \quad (6)$$

$$S_p = \int_0^\infty \frac{2}{r_p}\left[\frac{dV_p}{dr_p}\right] \cdot dr_p \quad (7)$$

Figure 5 illustrates the porosity distributions of BC (a) and BC (b) in comparison between water crystallization thermoporosimetry and B.H.J. nitrogen adsorption methods. The parameters derived from the porosity distributions in Fig. 5 are also listed in Table III. It is found that the calculation based on equation 2 yield pore sizes ranging between 12.6 and 37.1 nm that are within the valid pore size given by Landry (13). For both methods, the majority of pores tend to gather around an essentially the same particular size. The mean values (D_{av}) determined by thermoporosimetry are however slightly but non-significantly underestimated compared with B.H.J. nitrogen adsorption method i.e., D_{av} of 23.0 nm *vs.* 27.8 nm and 27.9 nm *vs.* 33.9 nm for BC (a) and BC (b), respectively, by thermoporosimetry *vs.* B.H.J. nitrogen adsorption. It is also found that V_p and S_p calculated by thermoporosimetry are underestimated especially for BC (b). It is noted that the volume of non-freezable water which was as high as 26% for water sorption in cellulose (7) is ignored in equations 6 and 7. This may bring the lack of agreement of the parameters derived between the two methods.

As seen in Fig. 5 and *S.D.* in Table III, the distribution from water crystallization thermoporosimetry are far narrower than that of B.H.J. In fact, thermoporosimetry using Gibb–Thomson equation gives the limited range of pore size determination. On one hand, it is set by thermodynamic assumptions that the process is no longer valid for temperatures lower than −40°C. As a result, the method is not able to characterize the pore size less than 2 nm. On the other hand, the upper limit is set by the effect of curvature on freezing point depression. For pores of 30 nm or larger the depressed temperature are so small that the effect cannot be separated from the free water fraction with satisfactorily accurate results (20). Many workers for examples, Isikiriyama *et al.* (15); Isikiriyama and Todoki (19); Landry (13); and Nedelec *et al.* (17) have used porous glasses of rigid wall to demonstrate the validity of the method. As cellulose fibrils are flexible in nature, upon freezing BC, only some of the pore wall with certain sizes might approach the same conditions as the porous glass systems that allow the pore analysis by thermoporosimetry to be essentially valid. And, freezing might also damage the pores (21). Thus, the crystallization of water confinement could be used as a probe for pore analysis with limitation, especially such a material containing soft pores as BC membrane under study. In addition, it is suggested that thermoporosimetry might not be suitable for determining an absolute measure but for gauging the porosity of one material against another (13).

CONCLUSION

In BC production by static culture of *A. xylinum*, different carbon sources could yield different sizes and crystal features of cellulose fibrils and reticulated porosities of the obtained film. The DSC thermal analysis revealed that a fraction of freezable bound water in BC presented in meta-stable state and behaved as a water confinement within pores rather than a solvent of cellulose polymer which is possible to use thermoporosimetry to approach pore structure of BC. However, the obtained porosity parameters may be underestimated due to a considerable non-freezable water fraction interacting with cellulose, and the validity of pore range based on thermodynamic assumptions of Gibb–Thomson effect.

ACKNOWLEDGEMENTS

The authors would like to thank Prince of Songkla University, Thailand Research Fund, and Commission on Higher Education for financial support. Special thanks also go to the Scientific Equipment Center, the Department of Pharmaceutical Technology, and the Department of Chemical Engineering for providing the lab facilities.

REFERENCES

1. H. S. BarudThermal characterization of bacterial cellulose–phosphate composite membranes. *J. Therm. Anal. Calorim.* **87**:815–818 (2007).
2. K. Watanabe, M. Tabuchi, Y. Morinaga, and F. Yoshinaga. Structural features and properties of bacterial cellulose produced in agitated culture. *Cellulose.* **5**:187–200 (1998).
3. D. Klemm, D. Schumann, U. Udhardt, and S. Marsch. Bacterial synthesized cellulose—artificial blood vessels for microsurgery. *Prog. Polym. Sci.* **26**:1561–1603 (2001).

4. T. Maneerung, S. Tokura, and R. Rujiravanit. Impregnation of silver nanoparticles into bacterial cellulose for antimicrobial wound dressing. *Carbohyd. Polym.* **72**:43–51 (2008).
5. G. Zografi and M. J. Kontny. The interactions of water with cellulose- and starch-derived pharmaceutical excipients. *Pharm. Res.* **3**:187–194 (1986).
6. D. Faroongsarng and P. Sukonrat. Thermal behavior of water in the selected starch- and cellulose-based polymeric hydrogel. *Int. J. Pharm.* **352**:152–158 (2008).
7. P. Luukkonen, T. Maloney, J. Rantanen, H. Paulapuro, and J. Yliruusi. Microcrystalline cellulose–water interaction—a novel approach using thermoporosimetry. *Pharm. Res.* **18**:1562–1569 (2001).
8. K. Gelin, A. Bodin, P. Gatenholm, A. Mihranyan, K. Edwards, and M. Strømme. Characterization of water in bacterial cellulose using dielectric spectroscopy and electron microscopy. *Polym.* **48**:7623–7631 (2007).
9. S. Hestrin, and M. Schramm. Synthesis of cellulose by *Acetobacter xylinum*: preparation of freeze dried cells capable of polymerizing glucose to cellulose. *Biotechnol. J.* **58**:345–352 (1954).
10. K. Sansernluk, S. Kaewnopparat, and D. Faroongsarng. Properties of bacterial cellulose produced by *Acetobacter xylinum* TISTR975 from different sugars and preparation of bacterial cellulose containing nanosilver. Proceedings 7th National Graduate Research Conference, Prince of Songkla University, Surat Thani, Thailand, 2007.
11. K. Nagamura, T. Hatakeyama, and H. Hatakeyama. Studies on bound water of cellulose by differential scanning calorimetry. *Tex. Res. J.* **51**:607–613 (1981).
12. V. D. Aleksandov and O. V. Sobol'. Comparison between superheating of crystals in melting and supercooling of melts in crystallization. *Russ. J. Phys. Chem.* **81**:2100–2103 (2007).
13. M. R. Landry. Thermoporosimetry by differential scanning calorimetry: experimental considerations and applications. *Thermochim. Acta.* **433**:27–50 (2005).
14. R. Neffati, L. Apekis, and J. Rault. Size distribution of water droplets in butyl rubber: application of DSC in thermoporosimetry. *J. Therm. Anal. Calorim.* **54**:741–752 (1998).
15. K. IshikiriyamaPore size distribution measurements of polymer hydrogel membranes for artificial kidneys using differential scanning calorimetry. *Thermochim. Acta.* **267**:169–180 (1995).
16. S. Park, R. A. Vanditti, H. Jameel, and J. J. Pawlak. Changes in pore size distribution during the drying of cellulose fibers as measured by differential scanning calorimetry. *Carbohyd. Polym.* **66**:97–103 (2006).
17. J.-M. Nedelec, J.-P. E. Grolier, and M. Baba. Thermoporosimetry: a powerful tool to study the cross-linking in gels networks. *J. Sol-Gel Sci. Techn.* **40**:191–200 (2006).
18. S. Ozeki. Dielectric properties of water adsorbed in slitlike micropores of jarosite. *Langmuir.* **5**:181–186 (1989).
19. K. Isikiriyama and M. Todoki. Pore size distribution measurements of silica gels by means of differential scanning calorimetry. *J. Colloid Interf. Sci.* **171**:103–111 (1995).
20. F. P. Cuperus, D. Bargeman, and C. A. Smolders. Critical points in the analysis of membrane pore structures by thermoporosimetry. *J. Memb. Sci.* **66**:45–53 (1992).
21. C. T. Maloney, H. Paulapurpo, and P. Stenius. Hydration and swelling of pulp fibers measured with differential scanning calorimetry. *Nord. Pulp Pap. Res.* **13**:31–36 (1998).